Clays and Clay Minerals, Vol. 54, No. 2, 209–219, 2006.

IDENTIFICATION OF NEOFORMED Ni-PHYLLOSILICATES UPON Ni UPTAKE IN MONTMORILLONITE: A TRANSMISSION ELECTRON MICROSCOPY AND EXTENDED X-RAY ABSORPTION FINE STRUCTURE STUDY

RAINER DÄHN[1,*], MICHEL JULLIEN[2], ANDRÉ M. SCHEIDEGGER[1], CHRISTOPHE POINSSOT[3], BART BAEYENS[1] AND MICHAEL H. BRADBURY[1]

[1] Laboratory for Waste Management, Paul Scherrer Institut, Villigen, CH-5232, Switzerland
[2] Commissariat à l'Energie Atomique, CEA-Cadarache, DEN/DTN/SMTM/LMTE F-13108 St Paul lez Durance Cedex, France
[3] Commissariat à l'Energie Atomique, CEA-Saclay, DEN/DPC/SCPA/LCRE, F-91191 Gif-sur-Yvette Cedex, France

Abstract—The aim of this work was to investigate whether neoformed Ni-phyllosilicates can be observed and identified using transmission electron microscopy (TEM) in combination with energy dispersive spectroscopy (EDS). The investigations focused on Ni-phyllosilicates formed from Ni-doped montmorillonite. The reaction conditions (pH 8, $[Ni]_{initial}$ = 660 and 3300 μM, 0.2 M $Ca(NO_3)_2$) employed were similar to those used in previous polarized extended X-ray absorption fine structure (P-EXAFS) investigations of neoformed Ni-phyllosilicates in a Ni-montmorillonite system.

The TEM investigations of Ni-doped montmorillonite revealed the presence of small, thin particles consisting of coherent stacks that yielded only three to five lattice fringes with spacings consistent with smectites. These small particles were neoformed phyllosilicates, based on the fact that the small particles were only observed in Ni-doped samples and their Ni content, as determined from EDS analysis, was high (up to 10 wt.% NiO). Furthermore, the particles did not possess the characteristic properties of montmorillonite particles, such as a 2:1 Si to Al ratio; instead these particles were rich in Si (up to 75 wt.% SiO_2). Unlike montmorillonite, these particles did not contain any Fe. The particles were also significantly more resistant to electron beam damage than montmorillonite particles, and EXAFS measurements confirmed the presence of neoformed Ni-phyllosilicates.

The TEM study further indicates the presence of a variety of additional minerals (*e.g.* cristobalite, halloysite) and an X-ray amorphous Si-rich phase. A Ni signal could only be detected in the latter phase at high Ni loadings (403 μmol/g), suggesting that Ni uptake at low metal loadings (<90 μmol/g) is mainly controlled by the neoformation of phyllosilicates.

Key Words—EXAFS, Montmorillonite, Neoformed Phyllosilicates, Ni, TEM.

INTRODUCTION

Using extended X-ray absorption fine structure (EXAFS) spectroscopy, it has been demonstrated that Ni-, Co- and Zn-containing precipitates can form when clay minerals and Al and Si (hydr)oxides are reacted with aqueous solutions containing Ni, Co and Zn, at initial metal concentrations below saturation of the pure metal (hydr)oxide forms (Towle *et al.*, 1997; Scheidegger *et al.*, 1998; Manceau *et al.*, 1999; Thompson *et al.*, 1999a; Thompson *et al.*, 1999b; Morton *et al.*, 2001; Schlegel *et al.*, 2001; Dähn *et al.*, 2002; Lee *et al.*, 2004). For example, Scheidegger *et al.* (1998) observed the formation of a Ni-Al layered double hydroxide (Ni-Al LDH) phase when pyrophyllite (a 2:1 clay mineral) was doped with Ni. The Ni-Al LDH phase formed after a contact time of only a few minutes, indicating that nucleation of the new phase occurs rapidly. Using polarized-EXAFS (P-EXAFS) Dähn *et al.* (2002) and Schlegel *et al.* (2001) showed the presence of neoformed phyllosilicates after treating di- and tri-octahedral 2:1 clay minerals (montmorillonite, hectorite) with Ni and Zn solutions at elevated pH and metal concentrations. The neoformed phases were oriented parallel to the octahedral smectite sheets (Schlegel *et al.*, 2001; Dähn *et al.*, 2002). In the case of Schlegel *et al.* (2001) a structural link of the neoformed phases to hectorite particles could be observed.

Investigations by TEM supported the evidence from EXAFS studies that precipitates formed upon metal uptake by clay minerals. For example, TEM was used to confirm the formation of a Ni-Al LDH phase upon Ni uptake in the presence of pyrophyllite (Scheidegger *et al.*, 1996b). The authors observed surface deposits on pyrophyllite particles doped with Ni at pH >7; these deposits were not present in the undoped sample and occurred preferentially along the edges of the pyrophyllite particles. Similarly, Thompson *et al.* (1999b) used TEM to discern the presence of a Co-Al LDH phase formed upon Co uptake in the presence of kaolinite (a 1:1 clay mineral) at pH 7.8. Nanometer-sized crystalline particles associated with the edges and basal surfaces of kaolinite were observed in the Co-doped material.

* E-mail address of corresponding author:
rainer.daehn@psi.ch
DOI: 10.1346/CCMN.2006.0540206

In this study, TEM imaging and energy dispersive spectroscopy (EDS) analysis were conducted to investigate whether Ni-phyllosilicates form in the presence of Ni-doped montmorillonite. The reaction conditions used in this study (pH 8, $[Ni]_{initial}$ = 660 and 3300 μM, 0.2 M $Ca(NO_3)_2$) were similar to those used in a previous P-EXAFS study which indicated neoformation of a Ni-phyllosilicate phase (Dähn *et al.*, 2002). In contrast to the previous experiments by Dähn *et al.* (2002), this TEM/EDS study was conducted with 'as received' montmorillonite without any further purification and conditioning procedures (untreated). Untreated montmorillonite was used since smectite particles in this material were more resistant to electron beam damage compared to those in purified and conditioned (Ca- and Na-treated) montmorillonite. The crystallinity of smectite particles of the treated samples suffered beam damage within <1 s, whereas the untreated material could withstand the electron beam for several seconds and up to 1 min. Complementary EXAFS measurements were performed with both untreated and treated montmorillonite to check whether the Ni-uptake mechanism (neoformation of a Ni-phyllosilicate) remained unchanged by using the untreated clay.

MATERIALS AND METHODS

Montmorillonite characterization

The STx-1 montmorillonite used was purchased from the Source Clays Repository of The Clay Minerals Society. X-ray diffraction (XRD) investigations of the 'as received' montmorillonite reveal the presence of minor quantities of calcite, quartz and kaolinite amounting to <~1 wt.%. For the TEM investigations, the untreated clay material was used, whereas EXAFS measurements were performed on both untreated and treated clay material. In the treatment process, the montmorillonite was washed thoroughly three times with 1 M $NaClO_4$ to produce Na-montmorillonite. The <0.5 μm size fraction was separated by repeated washing with de-ionized water, combined with centrifugation (600 g max., ~7 min) and decantation of the supernatant suspensions immediately followed by flocculation with 1 M $NaClO_4$ (Baeyens and Bradbury, 1997). Soluble hydroxy-Al compounds were removed by an acid treatment (pH 3.5, for 1 h) followed by neutralization (pH 7).

Conversion to Ca-montmorillonite was achieved by dialysis methods. Visking dialysis membranes (Medical Int., London) were partially filled with Na-montmorillonite suspensions, sealed and then agitated in a 1 L container filled with a 0.2 M $Ca(NO_3)_2$ solution. The background electrolyte was refreshed daily, and the procedure was continued until the electrical conductivity of the solution was equal to that of the original 0.2 M $Ca(NO_3)_2$. The final conditioned montmorillonite suspension was stored at 4ºC in the dark to minimize microbial growth.

The cation exchange capacity (CEC) of the untreated STx-1 montmorillonite is 844 meq kg^{-1} (Van Olphen and Fripiat, 1979). The CEC of the treated Ca-montmorillonite was determined to be 970 meq kg^{-1} by using the isotopic dilution method with ^{45}Ca (Baeyens and Bradbury, 1995). The external surface area of the untreated and treated STx-1 montmorillonite was measured by the N_2-BET technique to be 82 m^2g^{-1} and 89 m^2g^{-1}, respectively. These values are similar to that of 84 m^2g^{-1} given by Van Olphen and Fripiat (1979).

Sample preparation

The montmorillonite samples with low and high Ni loadings were prepared for analysis by TEM and EXAFS. Samples with low Ni loading were prepared by adding 0.64 g of the untreated STx-1 to 40 mL of a 0.2 M $Ca(NO_3)_2$ solution. The pH was adjusted to 8 and 60 mL of a Ni solution of 1100 μM (pH 8.0, 0.2 M $Ca(NO_3)_2$) was added, resulting in a solid to liquid ratio of 6.4 g/L and an initial Ni concentration ($[Ni]_{initial}$) of 660 μM. A previous study (Dähn *et al.*, 2002) demonstrated that the Ni solution was stable over a time period of up to 1 year and thus Ni uptake was not due to $Ni(OH)_2$(s) precipitation in this study. The high ionic strength $Ca(NO_3)_2$ background electrolyte was used to block Ni uptake on cation exchange sites. The experiments were conducted in a glove box under N_2 atmosphere (CO_2 and O_2 <2 ppm). The samples were centrifuged after reaction times of 14 (sample A; Table 1) and 60 days (sample B; Table 1). The supernatant solution was separated for analysis and the wet pastes were placed into Plexiglas holders, sealed and stored in a refrigerator to keep them moist prior to TEM and EXAFS measurements. The inductively coupled plasma-optical emission spectroscopy (ICP-OES) measurements of the supernatants showed that the quantity of Ni taken up varied from 43 μmol/g (sample A; Table 1) to 90 μmol/g (sample B; Table 1).

A sample with high Ni loading (sample C; Table 1) was prepared by adding 0.64 g of untreated STx-1 to 95 mL of 0.2 M $Ca(NO_3)_2$. The pH was adjusted to 8, and 5 mL of a Ni solution ($[Ni] = 6.6 \times 10^{-2}$ M, pH 3.0, 0.2 M $Ca(NO_3)_2$) were added. After 60 days of reaction the proportion of Ni taken up amounted to 403 μmol/g (sample C, Table 1).

An additional sample with a low Ni loading (sample D; Table 1) was prepared for EXAFS measurements using treated Ca-montmorillonite (<0.5 μm size fraction). Except for the solid to liquid ratio (5.2 g/L) the reaction conditions were identical to those described above for sample A (Table 1).

In addition to Ni, the supernatant solutions of the Ni-doped montmorillonite samples were also analyzed for Si and Al by ICP-OES (Table 1). The Al concentration in the samples was too low (<6 μM) to produce reliable ICP-OES measurements. The Si concentration in the

Table 1. Samples analyzed by TEM and EXAFS for untreated and treated Ni-doped montmorillonite.

Samples	Clay material	Clay treatment	Method	Solid/liquid ratio (g/L)	Ni uptake (%)	[Ni] (μmol/g)	Reaction time (days)	[Si] (μM)
A	montmorillonite	untreated	TEM, EXAFS	6.4	42[a]	43	14	406
B	montmorillonite	untreated	TEM	6.4	89[a]	90	60	527
C	montmorillonite	untreated	TEM	6.4	80[b]	403	60	488
D	montmorillonite	treated	EXAFS	5.2	32[a]	40	14	282

[a] Initial Ni concentration = 660 μM
[b] Initial Ni concentration = 3300 μM

Ni-doped montmorillonite samples varied between 282 and 527 μM.

TEM/EDS

The TEM investigations were performed using a JEOL 2000 FX transmission electron microscope operated at 200 kV at CEA-Cadarache in France. Energy dispersive spectroscopy (EDS) was performed using an Oxford Instruments Si-Li detector in convergent beam mode with a beam size of ~10 nm. The count time for the EDS analysis was 60 s with a deadtime of 0−10% and a count rate of 500 to 2000 counts/s. The detection limit of the EDS was 0.1 wt.% (Buseck and Self, 1992). The EDS data were semi-quantitatively analyzed using the program TEMQUANT from ISIS (Table 2).

The TEM/EDS samples were prepared by diluting a small amount of the centrifuged wet montmorillonite pastes in de-ionized water and by transferring a drop (10 μL) of the diluted suspension to a gold mesh grid with a holey carbon support film. The drop was then allowed to dry over 24 h in air at a temperature of 22ºC and a relative humidity of 70% prior to the TEM investigations.

EXAFS data collection and reduction

The Ni K-edge EXAFS spectra were obtained at the Swiss-Norwegian beamline (SNBL) at the European Synchrotron Radiation Facility (ESRF, Grenoble, France). All spectra were recorded in fluorescence mode at room temperature using a Si(111) monochromator and a Stern-Heald-type detector (Lytle detector, The EXAFS Co.). Higher-order harmonics were suppressed by using an Au-coated mirror. The monochromator angle was calibrated by assigning 8333 eV to the first inflection point of the K-absorption edge spectrum of Ni metal. Several EXAFS scans were averaged to improve the signal-to-noise ratio.

Data reduction was carried out with the WinXAS 3.1 software package (Ressler, 1998). The energy was converted to photoelectron wave vector units (Å^{-1}) by assigning the origin E_0 to the first inflection point of the absorption edge. Radial structure functions (RSFs) were obtained by Fourier transforming k^3-weighted $\chi(k)$ functions between 3.2 and 10 Å^{-1} using a Bessel window function with a smoothing parameter of 4. Amplitude and phase-shift functions were calculated with FEFF 8.0 (Rehr *et al.*, 1991) using the structures of β-$Ni(OH)_2$ and Ni-Talc (Perdikatsis and Burzlaff, 1981) as references. Fits were performed in R space in the 0.6 to 3.5 Å interval. The amplitude reduction factor (S_0^2) was determined to be 0.85 from the experimental β-$Ni(OH)_2$ EXAFS spectrum. The deviation between the fitted and the experimental spectra (%Res) is given by:

$$\%\text{Res} = \frac{\sum_{i=1}^{N} |y_{\text{exp}}(i) - y_{\text{theo}}(i)}{\sum_{i=1}^{N} y_{\text{exp}}(i)}$$

where N is the number of points in the fit window, and y_{exp} and y_{theo} are the experimental and theoretical RSF values. The precision for the bond distances (R) was

Table 2. EDS analyses of the montmorillonite samples A–C normalized to 100 wt.%.

	SiO_2	Al_2O_3	Fe_2O_3	NiO	MgO	CaO	Total
EDS1	94.28	4.45	0.24		0.59	0.44	100
EDS2	58.63	40.96			0.10	0.31	100
EDS3	92.94	4.94			1.2	0.92	100
EDS4	70.06	23.03	0.54		5.27	1.1	100
EDS5	70.65	21.60	0.27	1.09	4.07	2.32	100
EDS6	75.14	10.06		10.40	2.30	2.10	100
EDS7	64.10	19.51	0.48	9.08	4.54	2.29	100
EDS8	70.32	18.87		5.22	3.96	1.63	100
EDS9	58.65	39.85			0.66	0.84	100

previously estimated to be ±0.02 Å for R_{Ni-O}, and ±0.03 Å for R_{Ni-O} and R_{Ni-Si}, and ±0.5 for the coordination numbers (Dähn *et al.*, 2002).

RESULTS

TEM observations

Starting material. Before studying Ni-doped montmorillonite samples, we investigated the untreated clay material. The TEM observations demonstrated that the untreated starting material consisted mainly of smectite particles. However, additional mineral phases were identified. The variety of mineral phases present in the untreated montmorillonite material is demonstrated in Figure 1 in a low-magnification image. The image shows cauliflower-like features which are characteristic of cristobalite (cb) (Jackson *et al.*, 1977). Analysis by EDS showed that the cauliflower-like features consist of ~94 wt.% SiO_2 and ~4 wt.% Al_2O_3 (Table 2, EDS1), consistent with the composition of cristobalite (SiO_2; Strunz and Nickel, 2001). Based on the mineral morphology, the long (~900 nm) columnar particle at the right hand side of the image was identified as halloysite (ha) (Mitra and Bhattacherjee, 1975; Kirkman, 1981). Halloysite is a 1:1 clay mineral and is the hydrated form of kaolinite. The halloysite crystal had a fiber-like structure (diameter ~70 nm) and was hollow. The EDS analysis showed that the halloysite crystal consists of ~59 wt.% SiO_2 and ~41 wt.% Al_2O_3 (Table 2, EDS2). This finding is consistent with the structural formula of halloysite $(Al_4(OH)_8(Si_4O_{10}).2H_2O$; Strunz and Nickel, 2001). On the lower tip of the halloysite particle there was a diffuse and cloudy feature identified as an X-ray amorphous Si-rich phase consisting of ~94 wt.% SiO_2 and ~5 wt.% Al_2O_3 (Table 2, EDS3).

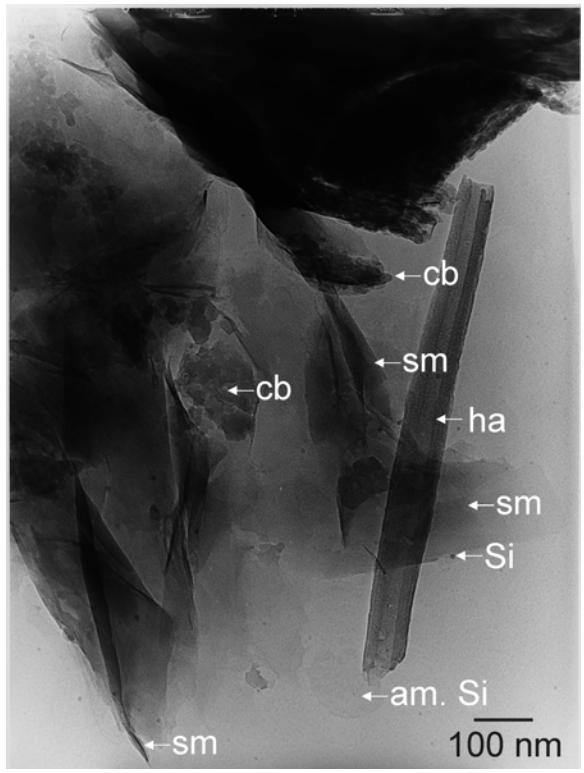

Figure 1. TEM image of different mineral phases in untreated montmorillonite. Only a few of the smectite particles (sm) observed in the image are labeled. The cauliflower-like features are cristobalite (cb), dark spots are clusters of Si (Si), the long particle is halloysite (ha) with an X-ray amorphous Si-rich phase (am. Si) at the lower tip.

An image of a smectite particle is presented in Figure 2a. At the lower edge of this particle, lattice fringes are visible (boxed areas in Figure 2). Lattice fringes are observed when the edges of smectite particles are curved upwards. If this is the case, the layers of smectite particles are parallel to the beam, allowing the observation of (001) lattice fringes. The lattice spacing of the illustrated particle (12 Å, Figure 2b,c) is characteristic of the spacing between (001) silicate layers in smectites (d_{001} = 12 Å, Meike, 1989; Allen, 1992). Only small areas of the smectite particle were in appropriate orientations to show clear lattice-fringe images (Figure 2b,c) indicating highly disordered stacking of the crystallites. The selected area electron diffraction (SAED) patterns of such intergrowths contained diffuse reflections resulting from a mixture of several disordered crystallites (Figure 2d; Peacor, 1992; Dong and Peacor, 1996). The EDS analysis showed that the core of the particle consists of ~70 wt.% SiO_2, ~23 wt.% Al_2O_3, ~0.5 wt.% FeO, ~5 wt.% MgO and ~1 wt.% CaO (Table 2, EDS4) which is consistent with montmorillonite. The montmorillonite particles in the untreated material were generally very fragile and suffered from radiation damage after exposing the sample to the electron beam for <1 min (*i.e.* the lattice fringes increasingly smeared out and finally disappeared). The image also shows the presence of an X-ray amorphous Si-rich phase (see above) associated with the smectite particle (dotted circled area in Figure 2).

Ni-doped montmorillonite. In the following we discuss whether TEM images and EDS analyses reveal any changes when the untreated clay material was doped with Ni. Sample B with low Ni loading consists of an assembly of smectite, cristobalite and halloysite particles and an X-ray amorphous Si-rich phase (Figure 3, Table 1). The TEM images show the presence of the same mineral phases as observed in the untreated material (Figure 1).

The EDS analysis of a series of cristobalite and halloysite particles and X-ray amorphous Si-rich phases did not detect any Ni signals in samples with low Ni loadings (samples A and B, Table 1). We could, however, obtain a Ni signal when smectite particles were analyzed. The textures from which these analyses

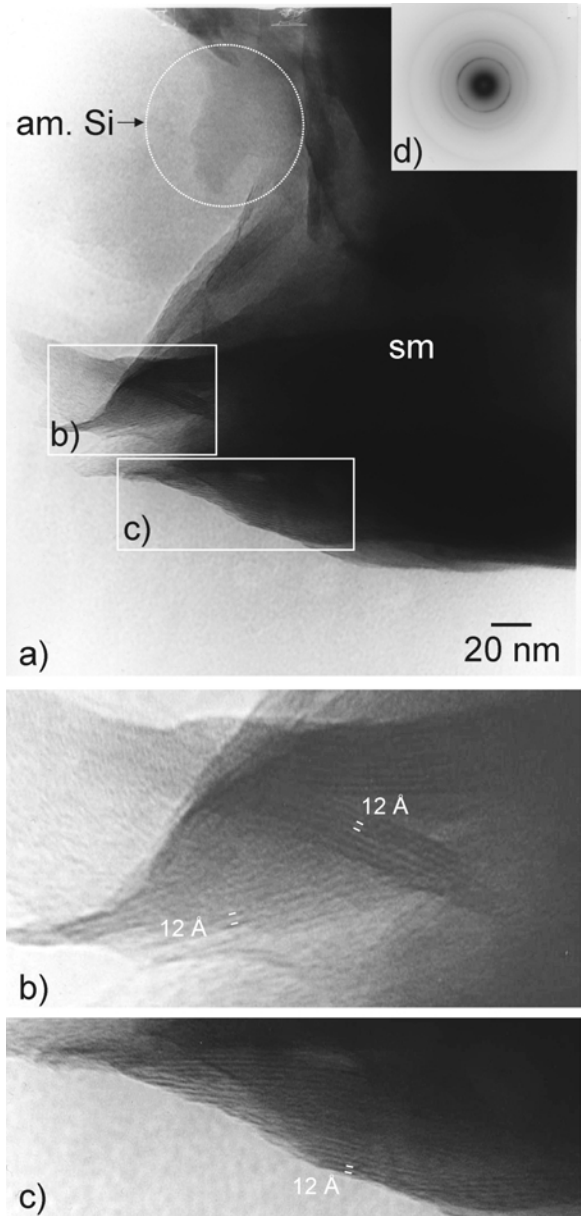

Figure 2. (a) Higher-resolution TEM image of a smectite (sm) in untreated montmorillonite with an X-ray amorphous Si-rich phase (am. Si, dotted circular area) and lattice fringes (boxed areas). (b,c) Magnified areas of Figure 2a. (d) SAED pattern of the smectite particle.

were obtained are shown in Figure 4. While the X-ray amorphous Si-rich phase and cristobalite contained no Ni, EDS analysis indicates that the center of the smectite (circled area) contained ~1 wt.% NiO (Table 2, EDS5).

Several montmorillonite particles contained a significantly larger Ni content (up to 10 wt.% NiO). The observed particles were generally very small and yielded only a few lattice fringes. Figure 5 shows a high-magnification image of particles (sm1, sm2, sm3) with 3–5 coherent lattice fringes (sample B, Table 1) and the

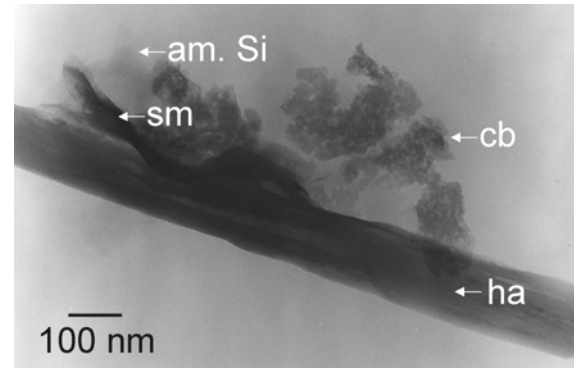

Figure 3. Halloysite crystal (ha), cristobalite (cb), X-ray amorphous Si-rich phases (am. Si) and smectite (sm) in a Ni-doped montmorillonite sample (90 µmol/g, 60 days' reaction time, sample B).

layer spacing of the lattice fringes in these particles is 11–12 Å, consistent with montmorillonites. Smectite particles with only a few lattice fringes were not observed in the starting material, suggesting that their appearance is related to the presence of Ni or a disruption of particles during exchange.

The EDS analysis of the very fine tip of sm3 (circled area in Figure 5) revealed that the tip of this smectite particle contained ~75 wt.% SiO_2, ~10 wt.% Al_2O_3 and ~10 wt.% NiO (Table 2, EDS6). The fact that the small particle (sm3) contained large amounts of NiO and SiO_2

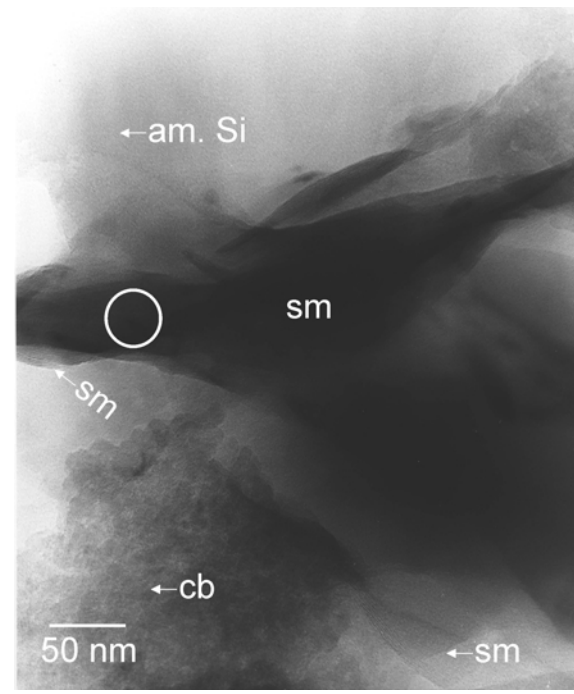

Figure 4. Smectite (sm), cristobalite (cb) and an X-ray amorphous Si-rich phase in a Ni-doped montmorillonite sample (43 µmol/g, 14 days' reaction time, sample A). The circled area marks the area of the EDS analysis of the smectite.

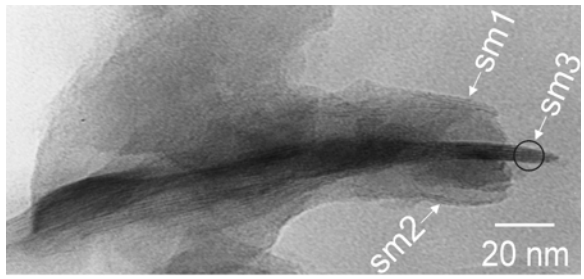

Figure 5. Neoformed phyllosilicate (sm1−sm3) in a Ni-doped montmorillonite sample (90 μmol/g, 60 days' reaction time, sample B). The circled area marks the area of the EDS analysis of sm3.

and relatively small amounts of Al_2O_3 demonstrates the presence of a Ni-rich silicate phase. The EDS analysis of the tip of sm3 further indicates that this smectite particle lacked Fe. For comparison, in the starting clay material, the Fe content in smectites, as measured by EDS, varied between 0.1 and 1 wt.%. A further characteristic of the Ni-rich small particles was their resistance to electron beam damage. While smectite particles in the starting material were generally very fragile and suffered from radiation damage after exposure to the electron beam for times of <1 min, the Ni-rich particles could withstand the electron beam for a much longer period (> 5 min).

The TEM/EDS investigations with samples having a high Ni loading (sample C, Table 1) again revealed no Ni signal from cristobalite and halloysite particles. In these samples, however, Ni was detected not only in the smectite, but also in the X-ray amorphous Si-rich phases. Figure 6 shows a high-magnification image of an X-ray amorphous Si-rich phase (circled area) sandwiched between two smectite regions. Whereas the tip of the lower smectite particle contained ~9 wt.% NiO (Table 2, EDS7), EDS data showed that the X-ray amorphous Si-rich phase contained ~5 wt.% NiO (Table 2, EDS8).

Figure 7 shows an image of a halloysite particle present in the Ni-doped material (sample A, 43 μmol/g, reaction time: 14 days). The EDS data analysis showed that the halloysite particle contained no detectable Ni (Table 2, EDS9). The diameter of the fiber is ~150 nm and exhibited holes with diameters of between 8 and 20 nm. No such holes occurred in halloysite particles in the starting material (Figure 1). Whereas halloysite particles were still observable when the material was doped with Ni at near neutral conditions for 14−60 days, no halloysite particles could be observed when the material underwent the purification and conditioning process (see the section on sample preparation).

EXAFS

A previous P-EXAFS study has shown unambiguously that Ni uptake in the presence of montmorillonite under similar reaction conditions resulted in the neoformation of a Ni-phyllosilicate (Dähn *et al.*,

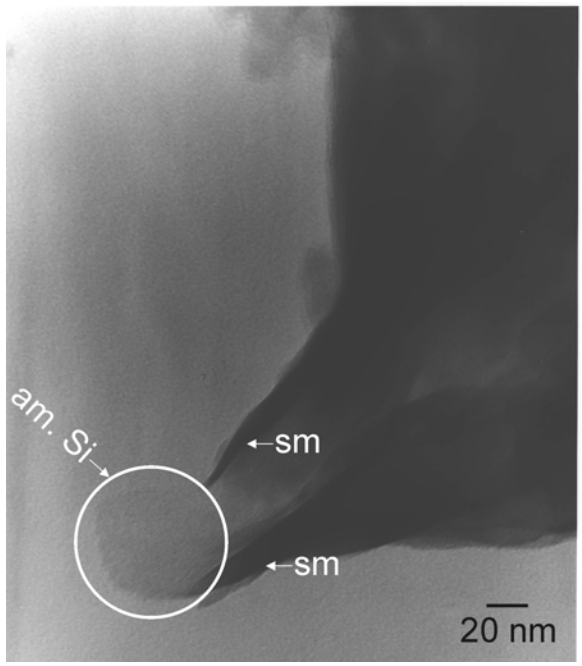

Figure 6. Smectite (sm) and an X-ray amorphous Si-rich phase (circled area) in a Ni-doped montmorillonite sample (403 μmol/g, 60 days' reaction time, sample C).

Figure 7. Halloysite crystal with core holes in a Ni-doped montmorillonite sample (43 μmol/g, 14 days' reaction time, sample A).

Table 3. Structural information derived from the EXAFS analysis using a three-shell fit approach for 14 days of reaction time ([Ni] = 43 μmol/g, sample A, untreated, and [Ni] = 40 μmol/g, sample D, treated montmorillonite).

	Ni−O			Ni−Ni			Ni−Si				
Sample	CN_{Ni-O}	R_{Ni-O} (Å)	σ^2 (Å^2)	CN_{Ni-Ni}	R_{Ni-Ni} (Å)	σ^2 (Å^2)	CN_{Ni-Si}	R_{Ni-Si} (Å)	σ^2 (Å^2)	ΔE_0 (eV)	%Res
Untreated	5.6	2.05	0.006	4.0	3.09	0.007	4.1	3.26	0.007[f]	0.6	3.6
Treated	5.7	2.05	0.006	3.1	3.09	0.006	3.5	3.28	0.006[f]	0.8	3.7

CN, R, σ^2, ΔE_o are the coordination numbers, interatomic distances, Debye-Waller factors and inner potential corrections.
[f]: fixed to the value obtained for Ni−Ni

2002). While in the previous Ni uptake study, treated montmorillonite (STx-1) was used, the TEM investigations here were performed with the untreated form of the same material.

We performed EXAFS experiments with Ni-doped untreated and treated montmorillonite to check whether the use of treated material modified the Ni uptake mechanism. The untreated material also contains particles >0.5 μm and minor minerals such as calcite, cristobalite, halloysite and X-ray amorphous Si-rich phases. The k^3-weighted EXAFS spectra for both montmorillonite samples doped with Ni at pH 8 for a reaction time of 14 days are shown in Figure 8 as an example (samples A and D, Table 1). The figure shows that the differences in the spectra attributable to the treatment procedure are minor. The multifrequency wave shape suggests the presence of at least two backscattering pairs. The corresponding experimental and the simulated Fourier transforms (FTs) are illustrated in Figure 9. The amplitude and position of the first RSF peaks (Ni−O contribution) do not differ in the two samples. The position of the second RSF peak for both samples is identical ($R + \Delta R \approx 2.75$ Å) and characteristic for Ni−Ni pairs (Manceau and Calas, 1986; Manceau, 1990; Pandya *et al.*, 1990; Scheidegger *et al.*, 1996a, 1997, 1998; Scheinost *et al.*, 1999; Mansour and Melendres, 1998; Dähn *et al.*, 2002). The amplitude of the second RSF peak, however, is slightly higher in the untreated sample compared to the treated sample.

Structural parameters obtained by data analysis are listed in Table 3. Data analysis indicates that the first shell consists of 5.6±0.5 Ni−O pairs at a bond distance (2.05 Å) which is typical of six-fold coordinated Ni (Pandya *et al.*, 1990). In both samples, Ni−Ni and Ni−Si distances were observed (R_{Ni-Ni} = 3.09 Å and R_{Ni-Si} = 3.26−3.28 Å) which match well with those in Ni-phyllosilicates (R_{Ni-Ni} = 3.05−3.09 Å, R_{Ni-Si} = 3.26−3.27 Å; Manceau and Calas, 1986; Charlet and Manceau, 1994; Dähn *et al.*, 2002). This finding confirms the formation of a Ni-phyllosilicate phase in both samples and that the use of the untreated clay did not modify the predominant uptake mechanism under the reaction conditions used.

DISCUSSION

Identification of Ni-phyllosilicates

The TEM images of both the starting material and Ni-doped montmorillonite demonstrated the presence of smectite particles with a shape and lattice fringes

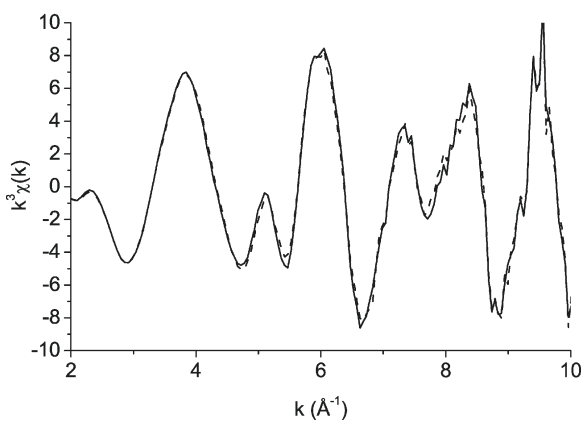

Figure 8. k^3-weighted Ni K edge EXAFS spectra of montmorillonite doped with Ni for 14 days for the untreated (solid line, [Ni] = 43 μmol/g, sample A) and the treated (dashed line, [Ni] = 40 μmol/g, sample D) clay material at pH 8.

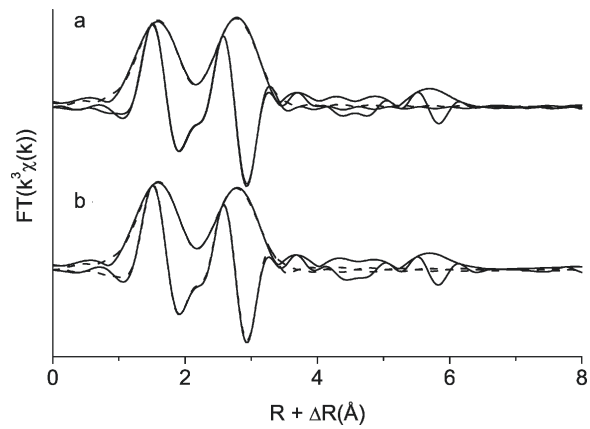

Figure 9. Experimental and theoretical Fourier transforms (modulus and imaginary parts, solid line: experimental data, dotted line: least-squares fit) obtained from the EXAFS spectra presented in Figure 8; (a) untreated and (b) treated.

characteristic of smectite (d_{001} = 12 Å; Meike, 1989; Allen, 1992). The *d* spacing varies with the hydration level and is 10 Å for a fully dehydrated smectite, and 15–20 Å for hydration levels between 10 and 50% (Kraehenbuel *et al.*, 1987). A lattice spacing of 12 Å refers to hydration levels of smectite particles between 5 and 10%. The study of Kraehenbuel *et al.* (1987) further demonstrated that a lattice spacing of 12 Å indicates the presence of one layer of water between smectite layers, whereas a lattice spacing of 15 Å is characteristic of two layers of water. Thus, although the TEM samples were measured under vacuum conditions in the TEM, a monolayer of water still remained in the interlayer of the smectites. The finding that lattice fringes were observable in the TEM images suggests that the crystallinity of the smectite particles did not significantly change during the Ni-uptake experiments.

In the Ni-doped clay material we also observed small, thin particles with only 3–5 lattice fringes (lattice spacing ~11–12 Å). There are several arguments indicating that these small particles (3–5 lattice fringes) are neoformed phyllosilicates. First of all, similar small particles were not observed in the starting clay material, and although these particles are very small in size, their Ni content (~10 wt.% NiO; sample B, Figure 5) is significantly higher than the average Ni content in the sample B of 0.7 wt.% NiO. The Ni content of these small particles is also significantly higher than that of the individual Ni-doped montmorillonite particles, which never exceeded 4 wt.% NiO (sample B). Furthermore, EDS analysis (Table 2, EDS6) confirmed that the Ni-doped montmorillonite particles are consistent with a structural formula for smectites (2:1 ratio of Si to Al), whereas the small particles are Si rich (~75 wt.% SiO_2) and Al poor (~10 wt.% Al_2O_3). Moreover, EDS analysis showed that the Fe content in the Ni-doped montmorillonite particles varied between 0.1 and 1 wt.% (FeO), while the small particles are lacking Fe. This finding is consistent with the total FeO content of the STx-1 montmorillonite (0.4 wt.%) (Dähn *et al.*, 2002) and is further evidence that these small particles were neoformed. Additional proof that the small particles were neoformed can be deduced from the fact that the small particles are significantly more resistant to electron beam damage than Ni-doped montmorillonite particles. Finally, the neoformation of a Ni-phyllosilicate is confirmed by the accompanying EXAFS measurements of this study which revealed structural parameters characteristic of Ni-phyllosilicates (Manceau and Calas, 1986; Charlet and Manceau, 1994; Dähn *et al.*, 2002).

Schlegel *et al.* (2001) investigated the uptake of Zn on hectorite and showed that neoformed phyllosilicates grow at the edges of smectite particles in continuity with the octahedral sheets. Using TEM we were not able to observe whether the neoformed Ni-phyllosilicates have a structural link with the montmorillonite particles. We observed small Ni-rich particles identified as neoformed phyllosilicates either close to or at larger distances from Ni-doped montmorillonite particles. This is similar to the TEM findings by Thompson *et al.* (1999b). Investigating Co uptake on kaolinite, these authors identified the presence of Co-Al LDH precipitates that were not preferentially oriented with respect to the kaolinite particles, and some of the precipitates had no contact with kaolinite particles.

Ni association with other mineral phases

In all Ni-doped montmorillonite samples (samples A–C, Table 1), a Ni signal could be detected when probing smectite particles, but none of the other minor mineral phases present in the sorbent material (*e.g.* halloysite and cristobalite) contained Ni. The detection of no Ni signal from halloysite, the hydrated form of kaolinite, indicates that the neoformed Ni-phyllosilicates are mainly associated with montmorillonite particles. The only exception to this finding were X-ray amorphous Si-rich phases, which were observed to be associated with smectite particles throughout this TEM study. While no Ni signal could be detected upon examination of the X-ray amorphous Si-rich phases in samples with a low Ni loading (samples A and B, Table 1), the presence of a Ni signal (up to 5 wt.% NiO) was detected in X-ray amorphous Si-rich phases in the sample with a high Ni loading (sample C, Table 1). The TEM/EDS findings thus indicate that Ni is primarily taken up by montmorillonite and neoformed Ni-phyllosilicates, and only a minor amount by the X-ray amorphous Si-rich phases.

It has been shown previously using EXAFS that Ni uptake on pyrophyllite and kaolinite at elevated Ni concentrations and pH resulted in the formation of a Ni-Al LDH phase (Scheidegger *et al.*, 1996a, 1996b, 1997). This TEM study confirms previous EXAFS studies demonstrating that Ni uptake on montmorillonite, pyrophyllite and kaolinite under similar reaction conditions results in the formation of different Ni phases (e.g. Scheidegger *et al.*, 1996a, 1996b, 1997; Dähn *et al.*, 2002). The precipitation of different Ni phases can be explained by different dissolution rates (Si release) of montmorillonite, pyrophyllite and kaolinite. Scheidegger *et al.* (1997) obtained Si release rates of 4.6×10^{-13} mol m^{-2} s^{-1} for Ni-doped pyrophyllite (pH 7.5, time range 0–216 h) and 5.2×10^{-12} mol m^{-2} s^{-1} for Ni-doped kaolinite (pH 7.5, time range 0–51 h). These Si release rates of Ni-doped pyrophyllite and kaolinite are at least one order of magnitude higher than the Si release rate of Ni-doped montmorillonite (3.5×10^{-14} mol m^{-2} s^{-1}, pH 8.0, time range 1–206 days; Dähn *et al.*, 2002). The higher dissolution rates of pyrophyllite and kaolinite cause the rapid formation of an X-ray amorphous Al hydroxide phase, which is a necessary precursor for the formation of Ni-Al LDH (Thompson *et al.*, 1999b; Yamaguchi, *et al.*, 2001). In the case of Ni-doped

montmorillonite, the dissolution rate is much smaller compared to pyrophyllite and kaolinite and therefore it seems that an X-ray amorphous Al hydroxide phase, which would favor the formation of a Ni-Al LDH, did not form. This hypothesis is supported by this TEM study, which observed only the precipitation of X-ray amorphous Si-rich phases, whereas Thompson *et al.* (1999b) observed in a TEM study of kaolinite the precipitation of X-ray amorphous Al-rich phases. This explanation is in line with the observed differences between Ni-doped montmorillonite and Ni-doped pyrophyllite/kaolinite. While the formation of Ni-AL LDH is rapid ($\geqslant$15 min) in Ni-doped pyrophyllite and kaolinite samples (Scheidegger *et al.*, 1996a, 1996b, 1997), the formation of a Ni-phyllosilicate in Ni-doped montmorillonite is much slower ($\geqslant$1 day; Dähn *et al.*, 2002). It thus appears that when X-ray amorphous Al-rich phases are present in the Ni-clay system, the rapid formation of Ni-LDH phases is preferential, whereas when not enough Al is available, the formation of Ni-phyllosilicates is favored.

Influence of the clay-purification and conditioning procedure

In metal-uptake experiments with montmorillonite, purifying and conditioning procedures are commonly applied in order to separate the clay fraction (<0.5 μm), to convert the clay into the homoionic form and to remove impurities and soluble hydroxy-Al compounds. We have conducted TEM observations with both untreated and treated montmorillonite to investigate whether the various treatment steps did modify the morphology of the clay material. We observed that the crystallinity of the smectite particles decreased significantly with each purifying and conditioning step and that the smectite particles became more prone to radiation damage, even when the sample was exposed to the electron beam for only seconds. For these reasons the TEM investigations were conducted with untreated clay material.

To investigate the influence of purification and conditioning on the uptake process, accompanying EXAFS measurements were performed with untreated as well as treated clay material. The EXAFS spectra were very similar, and in both cases the data analysis support the presence of a Ni-phyllosilicate phase (see the section on EXAFS and Table 3). This suggests that the purification and conditioning process did not modify the responsible uptake mechanism under the reaction conditions used.

Possible sources of Si in solution required for the neoformation of phyllosilicates

In a previous P-EXAFS study, Schlegel *et al.* (2001) observed the neoformation of a Zn-phyllosilicate phase upon treating hectorite with Zn. Whereas the reaction with Zn required the addition of Si, no Si addition was needed to form neophyllosilicates in the uptake of Ni onto montmorillonite (this study; Dähn *et al.*, 2002). The Si concentrations in this study (282−527 μM; Table 1) were comparable to those in the previous P-EXAFS study (177−448 μM, Dähn *et al.*, 2002) and were apparently sufficient for the neoformation of a Ni-phyllosilicate phase. Dähn *et al.* (2002) speculated that one reason for this distinct difference between the uptake mechanism of Zn on hectorite and Ni on montmorillonite was that the dissolution of SiO_2 particles in the sorbent material contributed to an increased $[Si]_{aq}$ in the latter case, thus facilitating the neoformation of Ni-phyllosilicate (this study, Dähn *et al.*, 2002). The TEM study demonstrated the presence of an X-ray amorphous Si-rich phase and thus confirms the above hypothesis. Another Si source observed in this study are halloysite particles. The TEM images suggest that halloysite particles suffer severe surface alteration during the experiments. The observed holes (Figure 7) are interpreted to be caused by partial dissolution of the halloysite particles during the Ni uptake experiment and thus halloysite particles represent a potential source of Al and Si in the system.

CONCLUSIONS

This study demonstrates that the uptake of Ni onto 'as-received' montmorillonite (pH 8, $[Ni]_{initial}$ = 660 μM) results in the formation of small Ni-rich particles which were identified as neoformed Ni-phyllosilicates by TEM observations. The finding that neoformed Ni-phyllosilicates are present in the Ni-doped montmorillonite sample was confirmed by EXAFS measurements. Furthermore, this study confirms previous P-EXAFS studies on the uptake of metal ions on clay minerals (Schlegel *et al.*, 2001; Dähn *et al.*, 2002) and demonstrates that neoformed phyllosilicates can be observed using TEM. Although TEM observations suggest that purification and conditioning of the clay material is a rather severe treatment, the main Ni uptake process (neoformation of phyllosilicates) did not change due to the treatment procedures commonly used. This finding implies that the results obtained in metal-uptake experiments with purified and conditioned clay minerals can be extrapolated to predict the fate of heavy metals in clay-rich natural settings.

ACKNOWLEDGMENTS

Experimental assistance from the staff of the Swiss-Norwegian Beam Lines at ESRF is gratefully acknowledged. The authors thank the European Synchrotron Radiation Facility (ESRF) at Grenoble, France, for the provision of beamtime. Dr E. Curti and M. Vespa are thanked for reviewing the manuscript. Partial financial support was provided by the National Co-operative for the Disposal of Radioactive Waste (Nagra), Wettingen, Switzerland. The handling of the manuscript by Dr P. Heaney and the constructive and helpful comments of Dr

M. Krekeler and an anonymous reviewer are gratefully acknowledged.

REFERENCES

Allen, F.M. (1992) Minerals definition by HRTEM: Problems and opportunities. Pp. 289–333 in: *Minerals and Reactions at the Atomic Scale: Transmission Electron Spectroscopy* (P.R. Buseck, editor). Reviews in Mineralogy, Vol. **27**, Mineralogical Society of America, Washington, D.C.

Baeyens, B. and Bradbury, M.H. (1995) A quantitative mechanistic description of Ni, Zn and Ca sorption on Na montmorillonite. Part I: Physico-chemical characterisation and titration measurements. PSI Bericht Nr. 95-10. Paul Scherrer Institut, Villigen, Switzerland and Nagra Technical Report NTB 95-04, Nagra, Wettingen, Switzerland.

Baeyens, B. and Bradbury, M.H. (1997) A mechanistic description of Ni and Zn sorption on Na-montmorillonite. Part I: Titration and sorption measurements. *Journal of Contaminant Hydrology,* **27**, 199–222.

Buseck, P.R. and Self, P. (1992) Electron energy-loss spectroscopy (EELS) and electron channeling (ALCHEMI). Pp. 289–333 in: *Minerals and Reactions at the Atomic Scale: Transmission Electron Spectroscopy* (P. R. Buseck, editor). Reviews in Mineralogy, **27**. Mineralogical Society of America, Washington, D.C.

Charlet, L. and Manceau, A. (1994) Evidence for the neoformation of clays upon sorption of Co(II) and Ni(II) on silicates. *Geochimica et Cosmochimica Acta* **58**, 2577–2582.

Dähn, R., Scheidegger, A.M., Manceau, A., Schlegel, M.L., Baeyens, B., Bradbury, M.H. and Morales, M. (2002) Neoformation of Ni phyllosilicate upon Ni uptake on montmorillonite: A kinetics study by powder and polarized extended X-ray absorption fine structure spectroscopy. *Geochimica et Cosmochimica Acta* **66**, 2335–2347.

Dong, H. and Peacor, D.R. (1996) TEM observations of coherent stacking relations in smectite, I/S and illite of shales: Evidence for MacEwan crystallites and dominance of $2M_1$ polytypism. *Clays and Clay Minerals,* **44**, 257–275.

Jackson, M.L., Clayton, R.N., Fuji, N. and Henderson, J.H. (1977) Cristobalite morphology and oxygen isotopic composition variation under hydrothermal alteration. *Clays and Clay Minerals*, **25**, 31–38.

Kirkman, J.H. (1981) Morphology and structure of halloysite in New Zealand tephras. *Clays and Clay Minerals,* **29**, 1–9.

Kraehenbuehl, F., Stoeckli, H.F., Brunner, F., Kahr, G. and Mueller-Vonmoos, M. (1987) Study of the water-bentonite system by vapour adsorption, immersion calorimetry and X-ray techniques: 1. Micropore volumes and internal surface areas, following Dubinin's theory. *Clay Minerals*, **22**, 1–9.

Lee, S., Anderson, P.R., Bunker, B.A. and Karanfil, C. (2004) EXAFS study of Zn sorption mechanisms on montmorillonite. *Environmental Science and Technology*, **38**, 5426–5432.

Manceau, A. (1990) Distribution of cations among the octahedra of phyllosilicates: Insight from EXAFS. *The Canadian Mineralogist*, **28**, 321–328.

Manceau, A. and Calas, G. (1986) Nickel-bearing clay minerals: II. Intracrystalline distribution of nickel: an X-ray absorption study. *Clay Minerals*, **21**, 341–360.

Manceau, A., Schlegel, M.L., Nagy, K.L. and Charlet, L. (1999) Evidence for the formation of trioctahedral clay upon sorption of Co2+ on quartz. *Journal of Colloid and Interface Science,* **220**, 181–197.

Mansour, A.N. and Melendres, C.A. (1998) Analysis of X-ray absorption spectra of some nickel oxycompounds using theoretical standards. *Journal of Physical Chemistry A,* **102**, 65–81.

Meike, A. (1989) Transmission electron microscope study of illite/smectite mixed layers. *NAGRA Technical Report*, **89–03**.

Mitra, G.B. and Bhattacherjee, S. (1975) The structure of halloysite. *Acta Crystallographica*, **B31**, 2851–2857.

Morton, J.D., Semrau, J.D. and Hayes, K.F. (2001) An X-ray absorption spectroscopy study of the structure and reversibility of copper adsorbed to montmorillonite clay. *Geochimica et Cosmochimica Acta*, **65**, 2709–2722.

Pandya, K.I., O'Grady, W.E., Corrigan, D.A., McBreen, J. and Hoffman, R.W. (1990) Extended X-ray absorption fine structure investigation of nickel hydroxides. *The Journal of Physical Chemistry*, **94**, 21–26.

Peacor, D.R. (1992) Diagenesis and low grade metamorphism of shales and slates. Pp. 335–380 in: *Minerals and Reactions at the Atomic Scale: Transmission Electron Spectroscopy* (P.R. Buseck, editor). Reviews in Mineralogy, **27**. Mineralogical Society of America, Washington, D.C.

Perdikatsis, B. and Burzlaff, H. (1981) Strukturverfeinerung am Talk $Mg_3[(OH)_2Si_4O_{10}]$. *Zeitschrift für Kristallographie*, **156**, 177–186.

Rehr, J.J., Mustre de Leon, J., Zabinsky, S. and Albers, R.C. (1991) Theoretical X-ray absorption fine structure standards. *Journal of the American Chemical Society*, **113**, 5135–5140.

Ressler, T. (1998) WinXAS: A program for X-ray absorption spectroscopy data analysis under MS-Windows. *Journal of Synchrotron Radiation*, **5**, 118–122.

Scheidegger, A.M., Lamble, G.M. and Sparks, D.L. (1996a) Investigations of Ni adsorption on pyrophyllite. *Environmental Science and Technology*, **30**, 548–554.

Scheidegger, A.M., Fendorf, M. and Sparks, D.L. (1996b) Mechanisms of nickel sorption on pyrophyllite: Macroscopic and microscopic approaches. *Soil Science Society of America Journal*, **60**, 1763–1777.

Scheidegger, A.M., Lamble, G.M. and Sparks, D.L. (1997) Spectroscopic evidence for the formation of mixed-cation hydroxide phases upon metal sorption on clays and aluminum oxides. *Journal of Colloid and Interface Science*, **186**, 118–128.

Scheidegger, A.M., Strawn, D.G., Lamble, G.M. and Sparks, D.L. (1998) The kinetics of mixed Ni-Al hydroxide formation on clay and aluminum oxide minerals: A time-resolved XAFS study. *Geochimica et Cosmochimica Acta* **62**, 2233–2245.

Scheinost, A.C., Ford, R.G. and Sparks, D.L. (1999) The role of Al in the formation of secondary Ni precipitates on pyrophyllite, gibbsite, talc, and amorphous silica: A DRS study. *Geochimica et Cosmochimica Acta*, **63**, 3193–3203.

Schlegel, M.L., Manceau, A., Charlet, L., Chateigner, D. and Hazemann, J.L. (2001) Sorption of metal ions on clay minerals. 3. Nucleation and epitaxial growth of Zn phyllosilicate on the edges of hectorite. *Geochimica et Cosmochimica Acta*, **65**, 4155–4170.

Strunz, H. and Nickel, E.H. (2001) *Strunz Mineralogical Tables*. Schweitzerbart'sche, Stuttgart, Germany.

Thompson, H.A., Parks, G.A. and Brown, G.E. Jr. (1999a) Ambient-temperature synthesis, evolution, and characterization of cobalt-aluminum hydrotalcite-like solids. *Clays and Clay Minerals*, **47**, 425–438.

Thompson, H.A., Parks, G.A. and Brown, G.E. Jr. (1999b) Dynamic interactions of dissolution, surface adsorption, and precipitation in an aging cobalt(II)-clay-water system. *Geochimica et Cosmochimica Acta*, **63**, 1767–1779.

Towle, S.N., Bargar, J.R., Brown, G.E. Jr. and Parks, G.A. (1997) Surface precipitations of Co(II) on Al_2O_3. *Journal of Colloid and Interface Science*, **187**, 62–82.

Van Olphen, H. and Fripiat, J.J. (1979) *Data Handbook for Clay Materials and Other Non-metallic Minerals.* Pergamon Press, New York.

Yamaguchi, N.U., Scheinost, A.C. and Sparks, D.L. (2001) Surface-induced nickel hydroxide precipitation in the presence of citrate and salicylate. *Soil Science Society of America Journal*, **65**, 729–736.

(*Received 21 December 2004; revised 21 November 2005; Ms. 991; A.E. Peter J. Heaney*)